GT2014-26249

LIP SEPARATION AND INLET FLOW DISTORTION CONTROL IN DUCTED FANS USED IN VTOL SYSTEMS

Ali Akturk *
Turbomachinery Aero-Heat Transfer Laboratory
Department of Aerospace Engineering
The Pennsylvania State University
University Park, Pennsylvania 16802
Email: akturkali@gmail.com

Cengiz Camcı[†]
Turbomachinery Aero-Heat Transfer Laboratory
Department of Aerospace Engineering
The Pennsylvania State University
University Park, Pennsylvania 16802
Email: cxc11@psu.edu

ABSTRACT

This paper describes a novel ducted fan inlet flow conditioning concept that will significantly improve the performance and controllability of ducted fan systems operating at high angle of attack. High angle of attack operation of ducted fans is very common in VTOL (vertical take off and landing) UAV systems. The new concept that will significantly reduce the inlet lip separation related performance penalties in the edgewise/forward flight zone is named DOUBLE DUCTED FAN (DDF). The current concept uses a secondary stationary duct system to control inlet lip separation related momentum deficit at the inlet of the fan rotor occurring at elevated edgewise flight velocities. The DDF is self-adjusting in a wide edgewise flight velocity range and its corrective aerodynamic effect becomes more pronounced with increasing flight velocity due to its inherent design properties. Most axial flow fans are designed for an axial inlet flow with zero or minimal inlet flow distortion. The DDF concept is proven to be an effective way of dealing with inlet flow distortions occurring near the lip section of any axial flow fan system, especially at high angle of attack. In this present paper, a conventional baseline duct without any lip separation control feature is compared to two different double ducted fans named DDF CASE-A and DDF CASE-B via 3D, viscous and turbulent flow computational analysis. Both hover and edgewise flight conditions are considered. Significant relative improvements from DDF CASE-A and DDF CASE-B are in the areas of vertical force (thrust) en-

hancement, nose-up pitching moment control and recovery of fan through-flow mass flow rate in a wide horizontal flight range.

NOMENCLATURE
β_1 Blade section inlet angle (deg)
β_2 Blade section exit angle (deg)
c Chord length (m)
c_1 Rotor inlet absolute velocity (m/s)
c_2 Rotor exit absolute velocity (m/s)
c_θ Tangential(swirl) component of the velocity (m/s)
c_x Axial component of the velocity (m/s)
D Overall diameter of the baseline ducted fan (m)
h Rotor Blade height(Rotor tip radius - Rotor hub radius)(m)
p Static pressure (pa)
ρ Density (kg/m^3)
ω Rotational Speed (radian/s)
r Radial distance measured from origin (m)
t Rotor tip clearance (m)
w_1 Rotor inlet relative velocity (m/s)
w_2 Rotor exit relative velocity (m/s)
X Axial coordinate measured from the inlet plane of the standard duct (m)
x x = X/c , non-dimensional axial distance

---

*Research engineer at Siemens Energy, Orlando,Fl
[†]Professor of Aerospace Engineering, ASME Fellow

INTRODUCTION

Ducted fan type propulsion offers an attractive solution by providing operational safety as well as compact vehicle/payload packaging. Ducted fans provide higher thrust to power ratio compared to free rotors as a result of diffusion of the propeller jet stream. When a VTOL ducted fan is in edgewise flight, because of the relative inlet flow dominantly normal to its axis of rotation, problems related to flow separation at the leading edge of the duct lip are encountered. This angle between the axis of rotation and inlet flow direction is usually termed as "*angle of attack*". At high angle of attack, the inlet flow separation leads to problems within the duct and may result in a high nose-up pitching moment as the edgewise flight speed is increased. Therefore, measuring and predicting the mean flow characteristics of ducted fans is crucial to understand the problems related to reliable and controllable horizontal flights.

Numerous studies have been undertaken in order to quantify the flow field characteristics around ducted fans. Experimental investigation has been one of the major approaches to study the flow characteristics of ducted fans. Abrego and Bulaga [1] performed wind tunnel tests to determine the performance characteristics of ducted fans for axial and edgewise flight conditions. Martin and Tung tested a ducted fan VTOL UAV with a 10-in diameter fan rotor [2]. They measured aerodynamic loads acting on the vehicle for different angle of attacks in hover and different crosswind velocities. They also included hot wire velocity surveys at inner and outer surface of the duct and across the downstream wake. The effect of tip gap on the thrust force produced was emphasized. They underlined the importance of tip vortex and duct boundary layer interaction. In addition, their study showed the effect of leading edge radius of duct on the stall performance and stability of the fan system. Graf *et al.* [3,4] improved ducted fan edgewise flight performance using a newly designed leading edge geometry which has been determined to be the significant factor in offsetting the effects of the adverse aerodynamic characteristics. Kriebel and Mendenball also carried out a theoretical and experimental study to predict ducted fan performance [5]. They developed methods for predicting the forces and moments on the duct, duct surface pressure distributions and boundary-layer separation. They have compared their predictions with measurements made on the Bell X-22A and Doak VZ-4 aircraft models. Their model qualitatively predicted the force and moment, the pressure distribution , and the separation of the boundary layer over the entire operating range of propeller thrust and free-stream angle of attack. Mort and Gamse [6] investigated aerodynamic characteristics of a seven foot diameter ducted propeller which was used on the Bell Aerosystems Company X-22A airplane. They reported aerodynamic characteristics for variations of power, free-stream velocity, blade angle, and duct angle of attack. Stall of both the upstream and downstream duct lips of this seven foot diameter ducted fan was examined as a function of angle of attack. Mort and Yaggy [7,8] performed hover and edgewise flight tests on a four foot diameter wing-tip mounted ducted fan that is used on Doak VZ-4-DA. Performance characteristics for the ducted fan were reported. They emphasized that pitching moment was rapidly changed and required power was increased due to separation, which occurred at windward side duct lip. They also reported that ducted fan supported by a fixed wing required less power in comparison to free flying ducted fan.

In addition to experimental studies, the ducted fan design and performance analyses were widely performed by using computational flow modeling. Lind *et al.* [9] carried out a computational study using a panel method. They compared their results to the experimental results from Martin and Tung [2]. He and Xin [10] developed the ducted fan models based on a non-uniform and unsteady ring vortex formulation. A numerical study in axial and horizontal flight conditions was conducted and validated with measured data. Chang *et al.* [11] developed an accurate grid generation methodology known as "*the curve adaptive option*" to model several industrial ducted fans. An axisymmetric, incompressible Navier-Stokes solver was implemented to calculate the flow field of a duct fan. The computational results agreed well with available wind tunnel data. Ahn *et al.* [12] applied a computational method to their ducted fan system to identify the design parameters which affect its performance. Ko *et al.* [13] developed a computer code aimed at the preliminary design of a ducted fan system. This code was validated using data from many wind tunnel and flight tests. It was also extensively used in the design of commercial ducted fans. Recently, Zhao and Bil [14] proposed a CFD simulation to design and analyze an aerodynamic model of a ducted fan UAV in preliminary design phase with different speeds and angles of attacks.

The motivation of this paper is to improve ducted fan flow characteristics by developing a novel inlet flow control and conditioning approach. This novel aerodynamic approach will also significantly improve the performance and controllability of VTOL UAVs and many other ducted fan based systems. The new concept that will measurably reduce the inlet lip separation related fan flow performance penalties in the edgewise flight zone is named "*DOUBLE DUCTED FAN (DDF)*". The current concept uses a secondary stationary duct system to control "*inlet lip separation*" at the inlet of the fan rotor, occurring at elevated edgewise flight velocities. The DDF is self-adjusting in a wide edgewise flight velocity range, in terms of its lip separation control ability. The following sections provide the detailed conceptual design approach of the DDF and its computational analysis. The DDF concept developed by the authors of this paper is also described in detail in a current U.S. Patent by Camci and Akturk [15] .

1 UPSTREAM LIP REGION FLOW PHYSICS FOR DUCTED FANS IN EDGEWISE FLIGHT

Ducted fan systems in edgewise flight at 90° angle of attack all inherently have an inlet flow direction that significantly deviates from the axis of the rotation. The inlet flow distortion near the leading side of all of these fan inlets becomes more problematic with increasing vehicle speed. The flow separation occurring on the inner side of the lip section severely limits the lift generation and controllability of VTOL UAVs. In general, the leading side of the fan near the lip separation zone breathes poorly when compared to the trailing side of the ducted fan. The trailing side total pressure is usually much higher than that of the near the leading side at the exit of the rotor. The flow near the leading side is adversely influenced by a separated flow zone that is characterized as highly re-circulatory, low momentum, unsteady and turbulent.

Conventional ducted fan systems also have a tip clearance loss that is proportional with the effective tip gap size. The specific shape of the tip region and the surface properties and arrangement designed onto the casing surface also influences the magnitude of tip clearance loss. This aerodynamic deficiency is measured as a significant total pressure loss near the tip at the exit of the rotor when the vehicle is only hovering with no horizontal flight. When the vehicle transits into a horizontal flight, the total pressure loss/deficit at the exit of the rotor near the leading side is much more significant than "*hover only*" loss of the ducted fan. In addition to the conventional tip clearance energy in mean kinetic energy, the rotor generates additional losses near the leading side, because of the re-circulatory low momentum fluid entering into the rotor near the tip section. This is clearly an off-design condition for an axial flow fan that is designed for a reasonably uniform inlet axial velocity profile in the spanwise direction. The immediate results of any inlet flow distortion entering into an axial fan rotor in edgewise flight are the loss of rotor's energy addition capability to the fluid near the leading side, an imbalance of the local mass flow rate between the leading side and trailing side and an imbalance of the total pressure observed at the rotor exit between the leading side and trailing side. A significant loss of lifting ability due to highly non-axisymmetric and unnecessarily 3D fan exit jet flow and unwanted nose-up pitching moment generation because the local static distributions imposed on the duct inner surfaces are typical flow characteristics for this common off-design operation at high angle of attack.

2 ADVERSE EFFECTS OF UPSTREAM LIP SEPARATION IN EDGEWISE FLIGHT

At high angle of attack, the onset of separation at the upstream duct lip is accompanied by the formation of a separation bubble. Existence of a significant separation bubble severely distorts inlet flow of the fan rotor especially near the leading side and in the tip clearance region. Distorted inlet flow causes an asymmetric loading of the ducted fan which increases the power required for level un-accelerated flight. The immediate results of operating a ducted fan in horizontal flight regime especially at high angle of attack are as follows:

Increased aerodynamic losses and temporal instability of the fan rotor flow when "*inlet flow distortion*" from "*the lip separation area*" finds its way into the tip clearance gap resulting the loss of "*energy addition capability*" of the rotor.

Reduced thrust generation from the upstream side of the duct due to the rotor breathing low-momentum and re-circulatory, turbulent flow.

A severe imbalance of the duct inner static pressure field resulting from low momentum fluid entering into the rotor on the leading side and high momentum fluid unnecessarily energized near the trailing side of the rotor.

A measurable increase in power demand and fuel consumption when the lip separation occurs to keep up with a given operational task.

Lip separation and its interaction with the tip gap flow requires a much more complex vehicle control system because of the severe non-uniformity of the exit jet in circumferential direction and excessive nose-up pitching moment generation.

At low horizontal speeds a severe limitation in the rate of descent and vehicle controllability may occur because of more pronounced lip separation. Low power requirement of a typical descent results in a lower disk loading and more pronounced lip separation.

Excessive noise and vibration from the rotor working with a significant inlet flow distortion.

Very complex unsteady interactions of duct exit flow with control surfaces.

3 DOUBLE DUCTED FAN CONCEPT

A novel ducted fan concept as a significant improvement over a standard ducted fan is illustrated in Figure 1. The poor edgewise flight characteristics of the reference duct as shown in Figure 1a are effectively improved with the "*Double Ducted Fan*" concept as presented in Figure 1b. A typical deficiency of a standard ducted fan is mainly related to the forward lip separation increasingly occurring when the edgewise flight velocity is gradually increased as shown in the streamline patterns of Figure 1a.

The inlet flow near the leading side of the standard duct is highly separated, low-momentum and turbulent. The apparent flow imbalance between the leading side and trailing side of the standard ducted fan as shown in Figure 1a causes an "*inlet-flow-distortion*". Flow simulations in Figure 1a show that the rotor barely breathes at the inlet section of the leading side although the trailing side passes a significant amount of flow. This flow
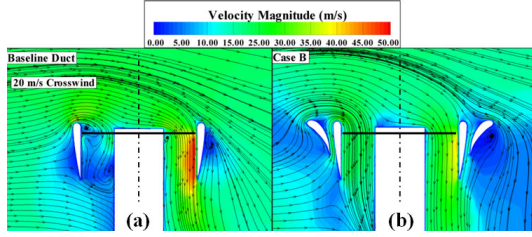
FIGURE 1: Separated flow near the forward lip section of a standard ducted fan (left) and the flow improvements from the novel concept Double Ducted Fan (DDF) at 9000 rpm, colored by the magnitude of velocity

imbalance amplified during the rotor "*energy adding process*" is one of the reasons of significant nose-up pitching moment generation. Figure 1b also presents the Double Ducted Fan (DDF) flow simulations indicating the effective inlet flow distortion reduction due to the unique aerodynamic properties of the new (DDF) system. The upstream lip separation near the leading side is almost eliminated resulting in a more balanced rotor exit flow field between the leading side and the trailing side. More detailed descriptions of the local flow field improvements resulting from the novel Double Ducted Fan (DDF) concept are discussed in the final part of this document. Although there may be many other potentially beneficial variations of the Double Ducted Fan concept, only the specific (DDF) form defined in Figure 1b will be explained in detail in the preceding sections.

3.1 Geometric Definition of a typical DDF arrangement

The DDF concept benefits from a second duct using a lip airfoil shape that has a much shorter axial chord length than that of the standard duct. The key parameter in obtaining an effective DDF arrangement is the size of the lip diameter D_L of the standard ducted fan. The second duct airfoil that is slightly cambered has a leading edge diameter set to 0.66 D_L as explained in Figure 2b. The angular orientation and axial position of the second duct airfoil is extremely important in achieving a good level of flow improvement near the leading side of the rotor. The leading edge circle of the second duct airfoil is slightly shifted up in the vertical direction for proper inlet lip separation control. The vertical distance between the duct inlet plane touching the standard duct and the plane touching the second duct is about $0.33D_L$ as shown in Figure 2b. The horizontal distance between the centers of the leading edge circles of the standard duct and outer duct is about $4D_L$. The axial chord of the second duct airfoil is about $5D_L$. The separation distance between the standard duct and second duct is controlled by the recommended throat width of $0.8D_L$ as shown in Figure 2b.

3.2 Converging-Diverging Channel in the Duct

The second duct and the standard duct forms a converging-diverging channel starting from the trailing edge of the second (outer) duct that is located at about $X=5D_L$. The axial position of the throat section is about 0.45c where c is the axial chord of the inner duct as shown in Figure 2b. The duct width at the entrance of the converging-diverging duct is D_L. The entrance to the converging-diverging channel is at the trailing edge point of the second duct. There is a (vertically up) net flow in the converging-diverging duct of the DDF. This flow is due to increasing dynamic pressure at the entrance of the converging-diverging duct at $X=5D_L$ when the edgewise flight velocity is increased. The diverging part of the channel flow between the standard and outer duct is extremely important in this novel concept, since this decelerating flow is instrumental in adjusting the wall static pressure gradient just before the lip section of the leading edge of the standard duct. The self-adjusting dynamic pressure of the inlet flow into the converging-diverging duct is directly proportional with the square of the edgewise flight velocity of the vehicle. The converging-diverging duct flow is in vertically up direction near the leading edge of the vehicle. The flow in the intermediate channel is vertically down when one moves away from the frontal section of the vehicle. This flow direction is caused by the relatively low stagnation pressure at the inlet of the intermediate channel at circumferential positions away from the leading edge. This vertically down flow induced by the static pressure field of the inner duct exit flow is likely to generate measurable additional thrust force for the DDF based vehicle.

4 VARIOUS POSSIBLE DOUBLE DUCTED FAN CONFIGURATIONS

The standard duct and three possible variations of the Double Ducted Fan (DDF) concept described in this study are presented in Figures 3 and 4. The vertical cross sections of the four duct configurations are included in these figures.

CASE-A as shown in Figure 3b is termed as the tall DDF. The tall DDF is able to generate a significantly higher thrust in hover position than that of the standard duct containing an identical rotor. However, in edgewise flight, due to the extended axial chord of the outer duct, the nose-up pitching moment generation is also significant in this design. This design has a throat section located at the trailing edge of the duct airfoils. Since the axial chord of the outer duct is longer than that of the inner duct this design may have a drag penalty when compared to the standard ducted fan.

Figure 4a shows the most effective Double Ducted Fan (DDF) configuration CASE-B since it has the ability to generate a significant amount of thrust when compared to that of the standard ducted fan configuration. Another important character-
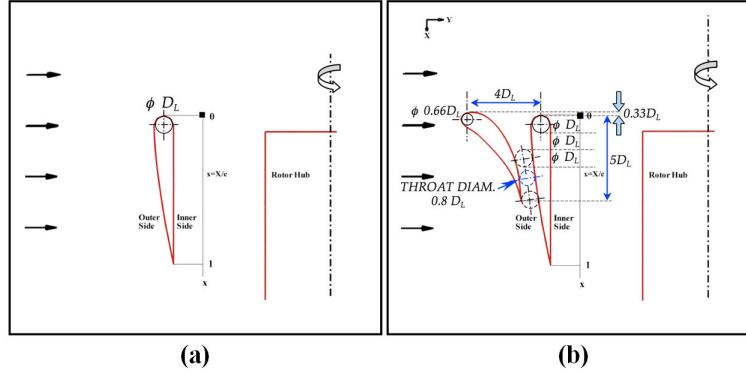
FIGURE 2: (a) Reference duct airfoil definition in a standard ducted fan arrangement, (b) Double Ducted Fan (DDF) geometry as a novel concept
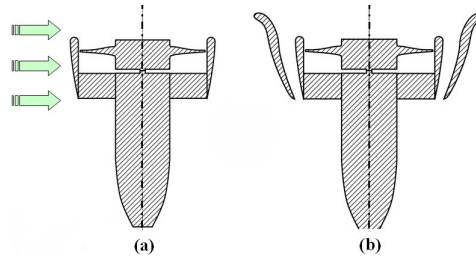

FIGURE 3: (a) Baseline ducted fan (Standard duct), (b) CASE-A tall double ducted dan (DDF)
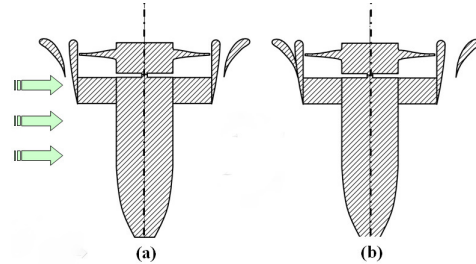

FIGURE 4: (a) CASE-B short double ducted fan, (b) Eccentric double ducted fan

istic of CASE-B is its ability to operate without enhancing the nose-up pitching moment of the vehicle in edgewise flight. This configuration was analyzed in great detail mainly because of its combined ability to enhance thrust and reduce nose-up pitching moment in edgewise flight without a significant drag increase.

An eccentric double ducted fan concept is also shown in Figure 4b. This concept requires a movable outer duct in order to control the throat area in the intermediate duct of the vehicle for a highly optimized edgewise flight performance.Variable throat mechanism introduced in this concept provides a greater range of operation in a DDF type vehicle offering a more accurate lip flow control over a much wider edgewise flight velocity range. Figure 4b shows a highly blocked second duct that is proper for

very low edgewise flight velocity. It is required that the throat area is enlarged by moving the outer duct as the edgewise flight velocity is increased. Although an almost optimal lip separation control can be achieved with an eccentric (DDF), its mechanical complexity and weight penalty is obvious. The outer duct airfoil definition of this concept is the same as CASE-B that is described in detail in Figure 2b.

5 DDF CONCEPT VALIDATION

A three dimensional simulation of the mean flow field around the ducted fan was performed using a custom developed actuator disk model based on radial equilibrium theory imple-

Rotor hub diameter		52 mm	
Rotor tip diameter		120 mm	
Blade height h		34 mm	
Tip clearance t/h		5.8 %	
Max blade thickness at rotor tip		1.5 mm	
Tailcone diameter		52 mm	
Tailcone length		105 mm	
Rotor blade section properties			
	Hub	Mid Span	Tip
Blade inlet angle β_1	60°	40°	30°
Blade exit angle β_2	30°	45°	60°
Blade chord	32 mm	30 mm	28 mm

TABLE 1: Geometric specifications of five inch ducted fan

mented into the commercial code Ansys-Fluent. The specific computational system solves the Reynolds Averaged Navier-Stokes (RANS) equations using a finite volume method.

5.1 Reference Ducted Fan Characteristics

The five bladed ducted fan rotor is driven by a brushless DC electric motor. This motor is speed controlled by an electronic speed control (ESC) system. The high efficiency electric motor driving the fan can deliver 1.5 kW power (2.14 HP) and spin at 1050 rpm per volt supplied to the motor. Figure 5 shows the five bladed reference fan that is used in the present DDF conceptual development effort. The relatively poor edgewise flight characteristics of the reference ducted fan shown in Figure 5 are significantly improved via the new double ducted fan (DDF) concept. The geometric specifications of the reference ducted fan unit that is designed for use in small scale uninhabited aircraft are presented in Table 1. This unit is manufactured from carbon composite material and has six outlet guide vanes at the exit of the fan in order to remove some of the swirl existing at the exit of the rotor. A tail cone is also used to cover the motor surface and hide the electrical wiring. All computational 3D flow simulations of the reference duct including the rotor flow field are performed at 9000 rpm using the geometry defined in Figure 5.

6 COMPUTATIONAL MODEL DESCRIPTION

A simulation of the mean flow field around and inside the ducted fan was performed by using a computational fluid dy-

namics code Ansys-Fluent [16]. The specific computational system solves the 3D Reynolds-Averaged Navier-Stokes equations using a finite volume method. The transport equations describing the flow field are solved in the domain that is discretized by using an unstructured computational mesh. The most complex and time consuming computational model is the modeling of unsteady/viscous/turbulent flow in and around the fan rotor by using an exact 3D model of rotor geometry using a sliding mesh technique. This type of solution is usually lengthy and requires significant computer resources especially in the edgewise flight mode when an axisymmetric flow assumption is not applicable. The current RANS computations use a custom developed rotor flow model termed as "*actuator disk model*" for the generation of the general inviscid flow features of the fan rotor. A k- ε turbulence model was invoked for the current computations, in areas other than the actuator disk.

6.1 Boundary Conditions

Hover: Figure 6 shows the specific boundary conditions and computational domain implemented in the solver for hover condition. The duct and tailcone surfaces are considered as solid walls with no-slip condition. On the side surfaces, a symmetry condition is assumed. For the hover condition, a pressure inlet boundary is assumed on the top surface. Atmospheric static pressure is prescribed on the top surface. Pressure inlet boundary is treated as loss-free transition from stagnation to inlet conditions. The solver calculates the static pressure and velocity at the inlet. Mass flux through boundary varies depending on interior solution and specified flow direction. Pressure outlet boundary condition is assumed on the bottom surface for hovering condition. Pressure outlet boundary interpreted as atmospheric static pressure of environment into which the flow exhausts. An additional custom developed "*Fan*" type condition was used for the implementation of the specific actuator disk model described in the next section.

Edgewise Flight: Figure 7 shows the specific boundary conditions implemented in the solver for edgewise flight. Like hover condition, the duct and tailcone surfaces are considered as solid walls with no-slip condition. Velocity inlet boundary condition is assigned on the windward side of the computational domain. Using this boundary condition velocity and turbulent intensity at the windward side is prescribed. For the leeward side of the domain an outflow condition is assigned. For the top, bottom and remaining side surfaces symmetry boundary condition is assigned. Like the hover condition, "*Fan*" type condition was set using a simplifed "*actuator disc model*" replacing the ducted fan rotor. Details of the inviscid actuator disk model is explained in the next section.
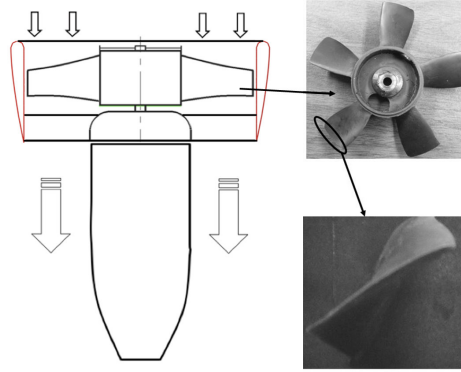
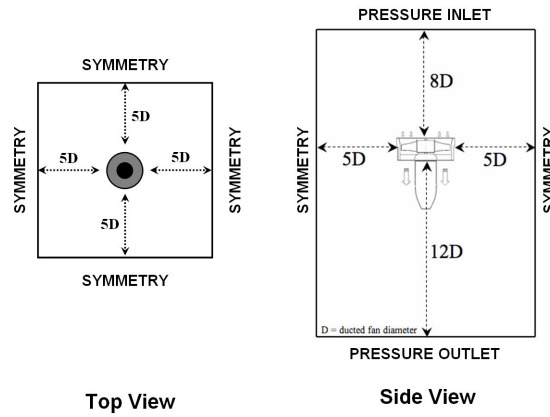**FIGURE 5**: Reference ducted fan and fan rotor used for DDF development effort

Top View

Side View

FIGURE 6: Boundary conditions for hover

6.2 Actuator Disk Model

The complex 3D rotor flow field in the rotating frame of reference is replaced by a simplified "*actuator disc model*" . This inviscid custom developed actuator disk model originates from the simultaneous use of the radial equilibrium equation, energy equation and the conservation of angular momentum principle across the fan rotor. The radial equilibrium equation is the force balance in the radial direction at a given axial position, balancing the pressure forces in radial direction with the centrifugal force. The viscous effects are ignored in this simplified and easy to implement "*actuator disc model*".

In this approach, a pressure change term is computed at each radial position of the rotor from hub to tip. The magnitude of the static pressure jump across the rotor is closely related to the amount of stagnation enthalpy change from the rotor inlet to exit. The stagnation enthalpy increase from the rotor inlet to exit is the same as the rate of energy provided to the fluid by the rotor per unit mass flow rate of the duct flow. The conservation of

angular momentum principle and energy equation suggests that the magnitude of this jump is mainly controlled by the tangential (swirl) component $c_{\theta 2}$ of the flow velocity in the absolute frame of reference at the exit of the rotor and rotor angular velocity.

Figure 8 presents the velocity triangles of the ducted fan rotor at inlet (1) and exit (2). β_1 and β_2 are the blade inlet and exit angles measured from the axial direction. Since the tip Mach number (0.28) of the rotor is not in the compressible flow range, it is reasonable to assume that the internal energy at the rotor inlet e_1 and exit e_2 is the same, $e_1 = e_2$. In a ducted fan rotor, it is realistic to assume that the "*axial component*" of the absolute velocity vector is also conserved from inlet to exit $c_{x2} = c_{x1}$. The flow is assumed to be axial at rotor inlet where $c_1 = c_{x1}$ and $c_{\theta 1} = 0$ under design conditions. The relative velocity vector at the exit of the rotor w_2 is smaller than the relative velocity w_1 at the rotor inlet. While the relative flow w_2 is diffusing in the relative frame of reference, the absolute flow velocity vector c_2 is accelerated at the rotor exit, because of added energy to the flow by the rotor.
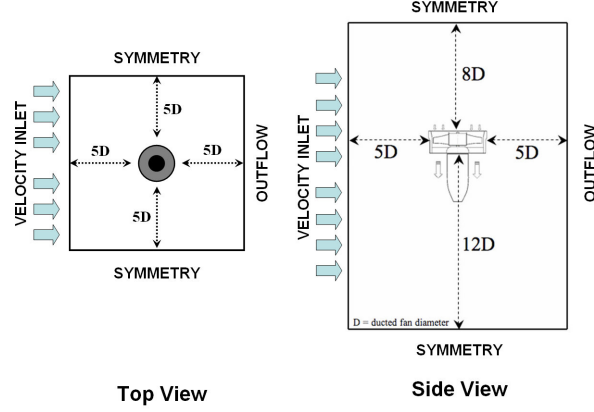
FIGURE 7: Boundary conditions for edgewise flight

	Fan Mass Flow Rate (kg/s)	Thrust (N)	Pitching Moment (N.m)	Flight Condition
Baseline Duct	0.30	3.04	0.00	No Crosswind (Hover)
Baseline Duct	0.29	3.47	0.17	10 m/s Crosswind
Baseline Duct	0.20	3.11	0.27	20 m/s Crosswind
MODIFIED DUCTS (DDF)				
CASE-A	—	—	0.00	No Crosswind (Hover)
CASE-A	0.31	4.93	0.37	10 m/s Crosswind
CASE-A	0.26	5.07	0.83	20 m/s Crosswind
CASE-B	—	—	0.00	No Crosswind (Hover)
CASE-B	0.30	3.72	0.16	10 m/s Crosswind
CASE-B	0.28	4.86	0.29	20 m/s Crosswind

TABLE 2: Computed rotor mass flow rate for all fan configurations during hover and edgewise flight

Equation 1 represents the change of stagnation enthalpy in the ducted fan rotor system. The right hand side of this equation is the rate of work per unit mass flow rate of air passing from the rotor. The right hand side is also the same as the product of the rotor torque and angular speed of the fan rotor.

$$h_{O2} - h_{O1} = U(c_{\theta 2} - c_{\theta 1}) \text{ where } U = \Omega r \text{ and } c_{\theta 1} = 0 \quad (1)$$

$$\left(h_2 + c_2^2/2\right) - \left(h_1 + c_1^2/2\right) = U c_{\theta 2} \quad (2)$$

$$\left(e_2 + \frac{p_2}{\rho_2} + c_2^2/2\right) - \left(e_1 + \frac{p_1}{\rho_1} + c_1^2/2\right) = U c_{\theta 2} \quad (3)$$

Equation 1 is a simplified form of the energy equation from rotor inlet to exit of a ducted fan unit. When $e_1 = e_2$ is substituted into equation 3 because of incompressibility condition, the "*Euler equation*" or "*pump equation*" results in as equation 4. Using equations 4 and 5, an equation for the calculation of static pressure jump between the rotor inlet and exit can be obtained.

The determination of $c_{\theta 2}$ is performed by using the velocity triangles in Figure 8. Since the blade inlet/exit angle distribution for 1 and 2 in radial direction is known from the existing rotor geometrical properties, shown in Table 1. w_2 can be calculated from the assumption that $c_{x2} = c_{x1} = c_1$. The absolute rotor exit velocity c_2 is determined by adding $U = \Omega r$ to w_2 in a vectorial
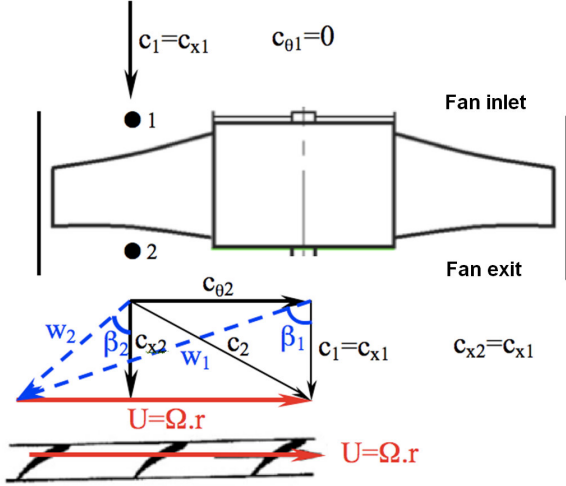
FIGURE 8: Velocity triangles at the inlet and exit of the ducted fan rotor

sense.

$$\frac{1}{\rho}\left(P_{O2} - P_{O1}\right) = U c_{\theta 2} \tag{4}$$

$$\left(p_2 + \rho \, c_2^2/2\right) - \left(p_1 + \rho \, c_1^2/2\right) = \rho U c_{\theta 2} \tag{5}$$

$$\Delta p = p_2 - p_1 = \rho \left[U c_{\theta 2} - \frac{1}{2}\left(c_2^2 - c_1^2\right) \right] \tag{6}$$

Equation 6 allows enforcing a prescribed pressure jump in function of density, radial position, rotor angular speed Ω, rotor exit swirl velocity $c_{\theta 2}$, c_1 and c_2. The rate of energy (per unit mass flow rate) added to the flow by the rotor is specified by the product $U c_{\theta 2}$ as shown in equations 4 and 5. Equation 6 could be evaluated at each radial position between the rotor hub and tip resulting in the radial distribution of the static pressure jump required by the general purpose viscous flow solver for a "*Fan*" type boundary condition. Δp can be effectively specified in a user defined function "*UDF*" in the solver. The "*Fan*" type boundary condition is an effective and time efficient method of implementing a rotor flow field via an "*actuator disk model*" in a 3D viscous flow computation.

6.3 Air Breathing Character of DDF in Edgewise Flight

Table 2 presents the computed fan rotor mass flow rate for all ducted fan types studied in this paper for both hover and edge-wise flight conditions. In addition to hover conditions, the results are also presented for 10 m/s and 20 m/s edgewise flight velocities at 9000 rpm rotor speed that is constant for all computations.

Flow simulations at constant rpm provide a basis for comparisons of 3D mean flow, fan thrust, nose-up pitching moment, total pressure and static pressure fields. Although the rotor speed is constant for all computations, the amount of mechanical energy transferred to the air during its passage through the rotor varies. This is mainly because of highly varying inlet flow field into the ducted fan unit during hover, edgewise flight at 10 m/s and 20 m/s. Table 2 also provides the computational estimates of thrust, nose-up pitching moment for hover and edgewise flight conditions.

Figure 9 shows that the baseline duct suffers from a high level of "*inlet flow distortion*" at 10 m/s and 20 m/s edgewise flight velocity. The overall mass flow rate passing from the ducted fan is reduced to 66 % of the hover mass flow rate as shown by the red line in Figure 9 (for 20 m/s edgewise flight). This significant limitation on the rotor mass flow rate is mainly the result of the large separated flow region occurring at just downstream of the lip section of the leading side of the duct as shown in Figure 1. While the leading side of the baseline duct passes a severely limited amount of air mass, the trailing side of the duct is able to breathe at a better rate than the leading side. It is apparent that the leading side of the baseline duct is partially blocked at high edgewise flight velocities. Figure 9 also shows a significant drop in rotor mass flow rate when the edgewise flight velocity is increased from 10 m/s to 20 m/s.

Baseline duct mass flow rate, thrust and nose-up pitching moment: Table 2 contains nose-up pitching moment information for all flight regimes showing a measurable increase in the pitching moment when the baseline vehicle moves at 10 m/s and 20 m/s in comparison to hover conditions. The nose-up pitching moment is measured with respect to the center of gravity of the ducted fan unit for all cases. At 20 m/s edgewise flight condition, the predicted pitching moment is 1.6 times that of the pitching moment at 10 m/s flight velocity. The pitching moment generation on a typical ducted fan in edgewise flight is directly related to the extent of inlet lip separation, the impingement of the rotor inlet flow on the duct inner surface (aft shroud surface) on the trailing side of the duct, imbalance of the rotor exit field between the leading side (low momentum) and trailing side (high momentum), aerodynamic profiling of the duct outer surface especially near the leading side.

Predicted baseline ducted fan thrust values at 10 m/s and 20 m/s increase to 1.5 times and 1.7 times of the thrust of the baseline duct at hover conditions. This relative thrust improvement is due to the specific external shape of the baseline duct and modified rotor inlet conditions at elevated edgewise flight speed levels.

Mass flow rate, thrust and nose-up pitching moment characteristics of CASE-A : The air breathing character of the
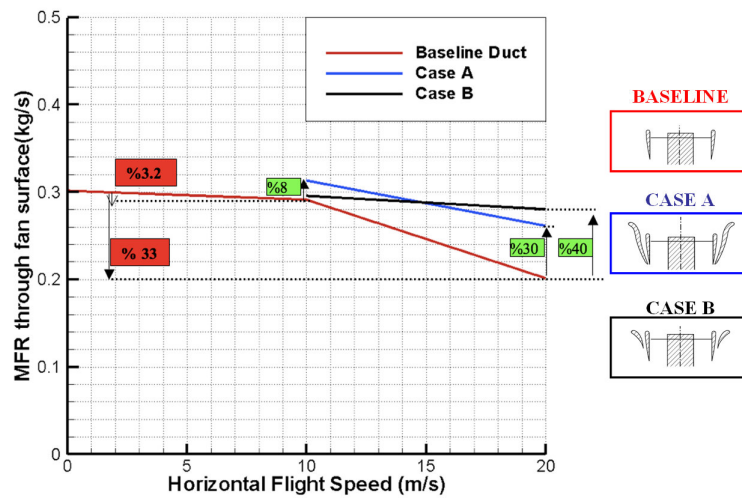
9

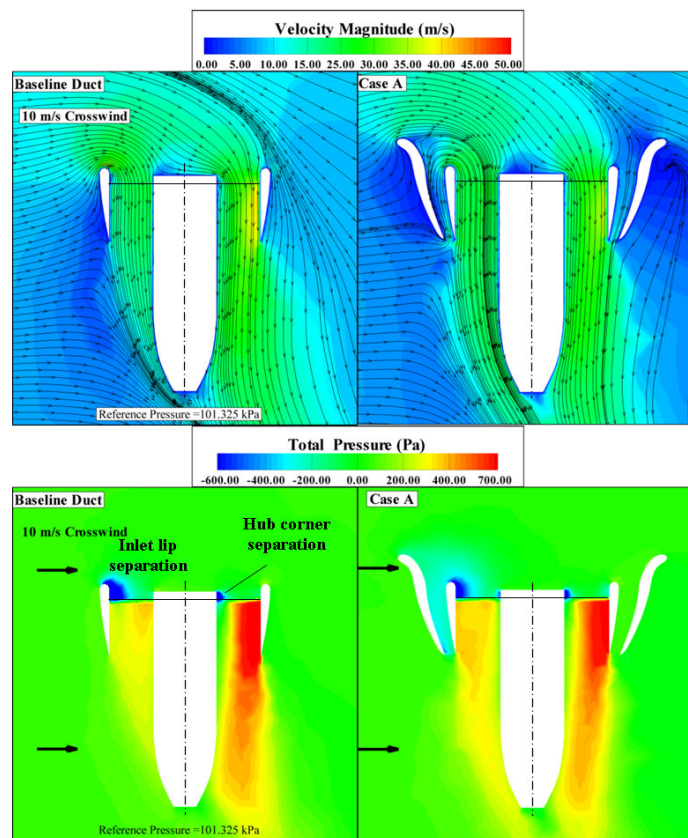**FIGURE 9**: Rotor disk mass flow rate versus edgewise flight speed at 9000 rpm

FIGURE 10: Velocity magnitude and total pressure distribution, baseline duct versus CASE-A double ducted fan (DDF) at 10 m/s edgewise flight velocity

baseline duct can be significantly improved by implementing the tall double ducted fan (DDF) designated as CASE-A as shown in Figure 9. The mass flow rate of CASE-A is about 8 % more than that of the baseline duct operating at the edgewise flight speed of 10 m/s. The rotor mass flow rate improvement for CASE-A at 20 m/s is much higher than that of the baseline duct operating at 20 m/s. A 30 % improvement over the baseline duct is possible. This relative mass flow rate improvement is a direct result of reduced inlet lip separation near the leading side of the duct designs at edgewise flight.

The predicted thrust for the tall double ducted fan (DDF) CASE-A is markedly higher than that of the baseline duct. At 10 m/s horizontal flight velocity, the thrust of CASE-A is about 1.7 times that of the baseline duct. When the flight velocity is elevated to 20 m/s, CASE-B produces an augmented thrust value of 1.9 times that of the baseline duct. The reduction of the inlet lip separation results in a direct improvement of the ducted fan exit flow near the leading side of the duct. The thrust improvements are due to both ducted fan exit flow improvements near the leading side of the unit, the external aerodynamic shape of the outer duct. The leading side of the DDF CASE-A rotor plane breathes air from the inlet at a much-improved rate than that of the trailing side. The tall (DDF) CASE-A also entrains a measurable amount of air into the outer duct from the inlet area of the unit especially near the trailing side. The flow in the outer duct is in opposite direction to the rotor flow near the leading side. However, the outer duct flow for the circumferential positions away from the leading side of the duct is in the same direction as the main rotor flow direction. Additional thrust augmentation is possible in the outer duct at positions away from the leading edge.

Although the tall (DDF) CASE-A is an excellent thrust producer at high edgewise flight velocities, it has the capability of augmenting the usually unwanted nose-up pitching moment mainly because of the external shape of the outer lip at elevated edgewise flight velocities. The pitching moment predicted at 10 m/s is about 2.2 times that of the baseline duct. At 20 m/s, the pitching moment produced by CASE-A is about 3.1 times that of the baseline duct value. The reason the short ducted fan CASE-B was designed and developed was the need to reduce the unwanted pitching up moment generation unique to CASE-A.

An effective DDF design CASE-B with highly reduced nose-up pitching moment: CASE-B as shown in Figure 9 is a shorter version of the double ducted fan design concept. CASE-B is designed to produce a significantly reduced nose-up pitching moment when compared to CASE-A. Another goal with CASE-B is to obtain similar thrust gains over the baseline duct. The short double ducted fan (DDF) CASE-B controls the lip separation as effectively as the tall (DDF) CASE-A without producing a high nose-up pitching moment. The airfoil geometry forming the outer duct has an axial chord length that is about half of the axial chord of the inner duct (also termed as standard fan or baseline fan). A detailed description of obtaining a short double

ducted fan (DDF) CASE-B is given in Figure 2a. starting from a baseline duct. Figure 9 indicates that the mass flow rate improvement (black line) of CASE-B is very similar to CASE-A (blue line). The short (DDF) CASE-B 's sensitivity to increasing edgewise flight velocity is much less when compared to tall (DDF) CASE-A. Implementation of a second duct as shown in Figure 2b enhances the lip separation controlled flight zone further into higher edgewise flight velocities. The thrust values predicted for the short (DDF) are much higher than the standard duct predictions at 10 m/s and 20 m/s. There is a slight reduction in thrust when comparison is made against the tall (DDF) CASE-A. The most significant property of CASE-B is its ability to control nose-up pitching moment effectively. The pitching moment generation for the short (DDF) CASE-B is very much suppressed when compared to tall (DDF) CASE-A. CASE-B nose-up pitching moments are about the same as the values predicted for the baseline duct. The short (DDF) concept described in Figure 6.b is a highly effective scheme of improving the lip separation related inlet flow distortion problem for the rotor of a ducted fan based VTOL vehicle. CASE-B is able to improve thrust without increasing the nose-up pitching moment generation. Since the leading side of the fan exit jet is well balanced against the trailing side of the exit jet, the effectiveness of the control surfaces at the exit of the ducted fan are expected to function much effectively for the short (DDF) CASE-B.

7 A COMPARATIVE EVALUATION OF LOCAL VELOCITY, STREAMLINES AND TOTAL PRESSURE FOR ALL THREE DUCTS

As part of the (DDF) concept validation, local flow field details including magnitude of velocity, streamlines and total pressure distributions are presented over a surface passing through the duct leading edge, axis of rotation and the trailing edge of the duct system. Comparisons of the specific (DDF) design against the corresponding baseline duct at 9000 rpm are discussed using the computational predictions explained in the previous paragraphs. The baseline duct; CASE-A, the tall DDF; and CASE-B, the short DDF results are compared in detail.

7.1 CASE-A Tall (DDF) versus Baseline Duct Results /at 10 m/s and 20 m/s

Figure 10 compares the flow fields of tall double ducted fan designated as CASE-A and the baseline duct. A slight forward lip separation is observed at 10 m/s edgewise flight velocity. The tall double ducted fan CASE-A produces an enhanced thrust level of 1.73 times that of the baseline ducted fan at 10 m/s. The mass flow rate of CASE-A at 9000 rpm is also enhanced when compared to the baseline ducted fan, as shown in Figure 10. The total pressure distributions clearly show the low momentum regions due to inlet lip separation and hub corner separation on the
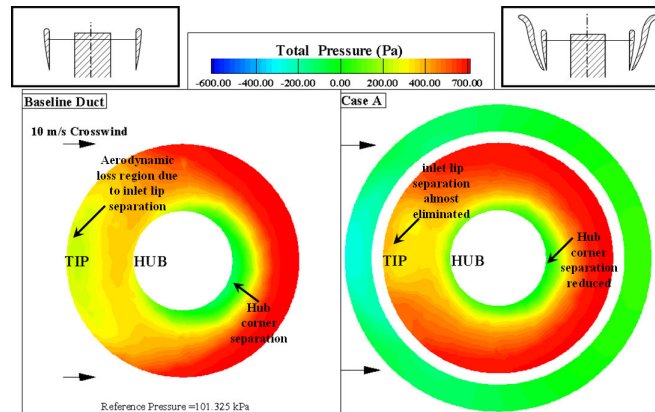
FIGURE 11: Total pressure distribution at rotor exit plane (horizontal) baseline duct versus CASE-A tall double ducted fan (DDF) at 10 m/s edgewise flight velocity
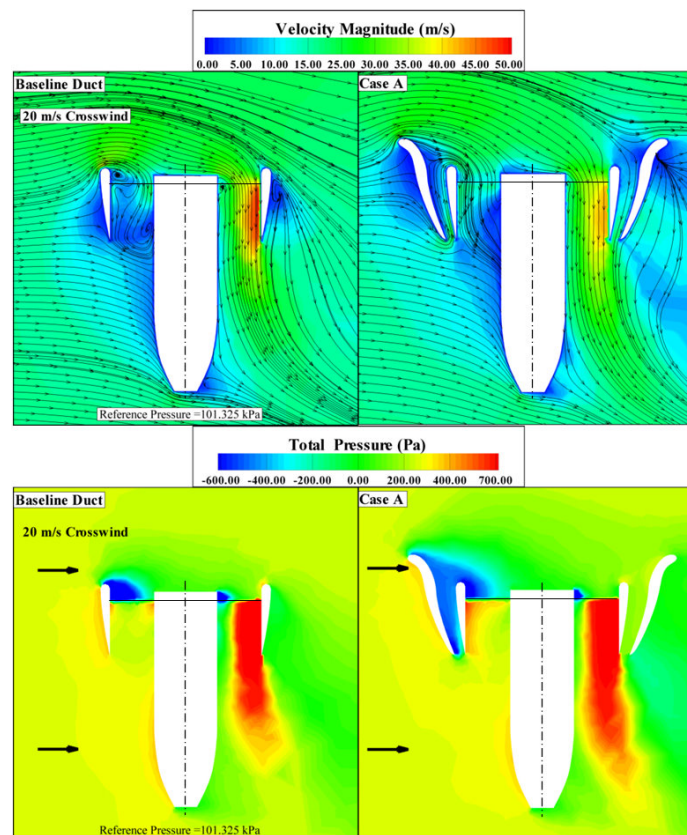

FIGURE 12: Velocity magnitude and total pressure distribution, baseline duct versus CASE-A tall double ducted fan (DDF) at 20 m/s edgewise flight velocity
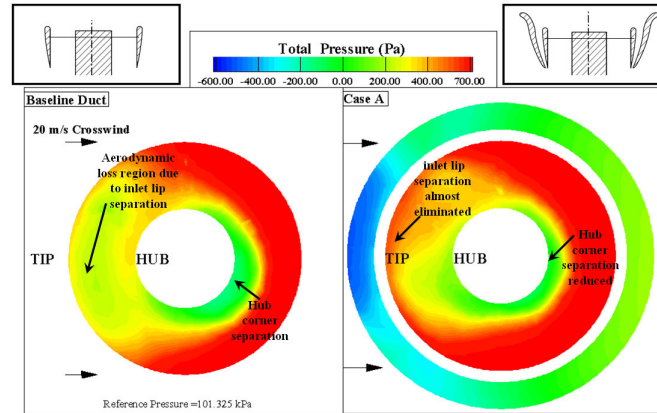
FIGURE 13: Total pressure distribution at rotor exit plane (horizontal) baseline duct versus CASE-A tall double ducted fan (DDF) at 20 m/s edgewise flight velocity

rotor disk inlet surface as shown by dark blue areas in Figure 10. The tall ducted fan provides a reduction in the size of the low momentum flow areas downstream of the inlet lip and hub corner when compared to the baseline duct.

Although the "*hub corner separation*" area is relatively smaller than the "*inlet lip separation*" area, the flow blockage created by the hub corner separation affects the flow downstream of the rotor as shown in Figure 10. The total pressure imbalance observed at downstream of the rotor for the baseline duct is significant. The existence of the tall double ducted fan CASE-A slightly improves the total pressure on the leading side of the rotor exit flow for 10 m/s edgewise flight velocity.

Figure 11 explains the effect of inlet flow distortion existing in the baseline duct and tall double ducted fan design at 10 m/s edgewise flight velocity by using rotor exit total pressure predictions. The light green zone near the leading side of the baseline ducted fan shows the highest level of aerodynamic loss resulting from "*inlet lip separation*" at 10 m/s. This area is where the relative flow tends to separate because of the existence of the duct lip near the leading side. The fan inlet surface also has another aerodynamic loss region (green) at just downstream of the "*hub corner*" on the trailing side of the duct. The beneficial influence of the tall double ducted fan design CASE-A is shown in Figure 11. The aerodynamic loss areas in the baseline duct distribution are effectively reduced in the tall double ducted fan design. The red total pressure zone near the trailing side of the baseline duct shows the highest levels of total pressure over the rotor exit plane. The trailing side tends to pass most of the inlet mass flow rate including the fluid that is skipping over (deflected by) the lip separation region. This is a common observation in most standard ducted fans in horizontal flight.

The aft part of the fan usually generates additional drag force because of this red high total pressure zone at the exit plane. The implementation of the tall double ducted fan makes the total pres-

sure distortion between the leading side and trailing side much more balanced. The inlet flow distortion is efficiently dealt with with the implementation of the second duct configuration termed as CASE-A, Figure 11.

When edgewise flight velocity is increased to 20 m/s, Figure 12 shows the highly adverse character of the separated flow zone behind the inlet lip section in the baseline duct. The flow also tends to separate behind the hub corner on the trailing side of the duct. Figure 12 demonstrates that the flow is nearly blocked by the existence of a large separated flow zone and the flow is effectively induced into the trailing side of the duct. The imbalance in the local mass flow rate between the leading side of the duct and the trailing side of the duct at 20 m/s is much more apparent when compared to 10 m/s results. Figure 12 displays the significant flow improvement in the lip separation area for the tall double ducted fan (DDF) CASE-A. The re-circulatory flow is almost eliminated downstream of the lip. The leading side of the duct starts breathing effectively because of CASE-A's ability to eliminate inlet flow distortion near the leading side. The (DDF) CASE-A results show a low momentum region that could be viewed as a three dimensional wake region behind the vehicle at 20 m/s edgewise flight velocity. The outer duct flow near the leading side is in a direction opposite to rotor flow direction. The outer duct flow near the leading side is an essential component of the (DDF) concept because of its highly important role in reversing the inner lip region separated flow conditions. The outer duct flow smoothly reverses into the rotor flow direction away from the leading side.

The rotor exit plane total pressure distribution shown in Figure 13, (DDF) CASE-A reveals a significant lip separation improvement leading to a much uniform inlet flow distribution between the leading side and trailing side of the inner duct. The DDF duct local flow distribution at the rotor exit is much improved in comparison to the baseline duct. Hub corner separation

area is also reduced in (DDF) CASE-A. Most circumferential positions of the second duct (other than the leading side of the duct) contributes to the generation of thrust because of the measurable outer duct flow observed in this area.

7.2 CASE-B Short (DDF) versus Baseline Duct Results at 10 m/s and 20 m/s

Figures 14 and 15 show the most effective double ducted fan (DDF) treatment results obtained for a edgewise flight velocity of 10 m/s. A detailed geometrical definition of the short double ducted fan (DDF) CASE-B was discussed in Figure 2b.

The short DDF has the ability to improve thrust in relative to the baseline case "*without producing a significant nose-up pitching moment*" by effectively reducing inlet lip separation and hub corner separation areas. The short double ducted fan configuration is a self adjusting lip separation control system preserving its separation control features in a wide range of edgewise flight velocities. The effectiveness of the short DDF treatment is shown in the total pressure distribution presented in Figure 14 for 10 m/s flight velocity. In addition to the area reduction of the separated flow areas (dark blue), the total pressure imbalance between the leading side and trailing side is almost eliminated. The leading side of the inner duct of the short DDF CASE-B breathes at a much improved rate as compared to the baseline case. The red high total pressure areas provide a well-balanced fan exit jet near the leading side and trailing side of the fan.

Figure 15 indicates a high level of rotor exit total pressure uniformity for CASE-B in contrast to the strong flow distortion generated by the baseline duct. When short double ducted fan is used, the lip separation and hub corner separation control is highly effective at 10 m/s flight velocity. The level of total pressure values between the leading side and trailing side are much better balanced in CASE-B as shown in Figure 15.

When the short double ducted fan arrangement (DDF) CASE-B is evaluated at 20 m/s flight velocity, the loss elimination features near the leading side lip, hub corner area are much apparent. Highly separated lip region flow adversely blocking the leading side of the inner duct is successfully dealt with the flow control features of the short (DDF) as shown in Figure 16. A well-balanced short (DDF) exit flow provides a higher level of thrust when compared to the baseline duct. The flow improvements and thrust enhancement from the short (DDF) comes with no additional nose-up pitching moment generation when compared to baseline as explained in Table 2 and Figure 16. A highly effective inlet flow distortion control ability of the short ducted fan can be apparently seen in Figure 17. A vehicle using the short (DDF) concept CASE-B generates a higher level of thrust with a well balanced ducted fan exit flow without excessive generation of nose-up pitching moment. This approach results in improvements of the performance of the control surfaces and improved range because the energy efficiency of the ducted fan is

improved. The elimination of severe inlet flow distortion is likely to improve the rotor exit flow quality before further interaction with typical control surfaces.

8 UPSTREAM LIP REGION LOCAL FLOW IMPROVEMENTS IN (DDF)

Figure 18 defines the local sampling locations for static pressure and skin friction coefficient computations on the airfoil of the inner duct at the leading edge location. The lowercase characters represent the "*rotor side*" locations and the uppercase characters show the "*outer side*" sampling locations for static pressure and skin friction coefficient on the inner duct airfoil section. The "*outer side*" denotes the channel between the baseline duct and secondary duct.

8.1 Static Pressure Distribution around the Lip Section of the Baseline Duct

Figure 19 shows the static pressure distribution for the baseline duct and double ducted fan (DDF) CASE-B for the edgewise flight velocity of 20 m/s. The distributions presented in Figure 19 are plotted around the airfoil of the baseline duct. The pressure gradient occurring around the leading edge radius of the inner duct is the most significant parameter controlling severeness of the leading edge lip separation problem. Point x=X/c=0 shows the leading edge and x=X/c=1 shows the trailing edge location of the baseline duct airfoil. The external flow stagnates on the the baseline duct airfoil at point D as shown in Figure 19 . The approaching flow to the duct is divided into a stream reaching up to the leading edge and a second stream approaching down to the trailing edge of the duct airfoil at point D. The static (or stagnation) pressure from point D to J remains almost constant. The external flow slightly accelerates to the leading edge point from point C to A for the baseline duct. There is a strong acceleration zone between point A and the leading edge point O, as clearly shown by the favorable pressure gradient between the point A and O. This is the area within the leading edge diameter of the inner lip section. The geometrical leading edge point O is the minimum pressure point for the baseline duct airfoil. The flow on the inner side of the lip sees a very strong adverse pressure gradient around the leading edge circle. The strong flow separation character shown in Figure 19 is mainly due to the strong adverse pressure gradient affecting the boundary layer growth between points O, a and finally b. The rotor process described in equations from 1 to 6 results in the sudden pressure rise on the inner part of the baseline duct between b and c.

8.2 Static Pressure Distribution around the Lip section of the Double Ducted Fan (DDF)

Figure 19 also shows the static pressure distribution around the lip section of the short double ducted fan (DDF) CASE-B.
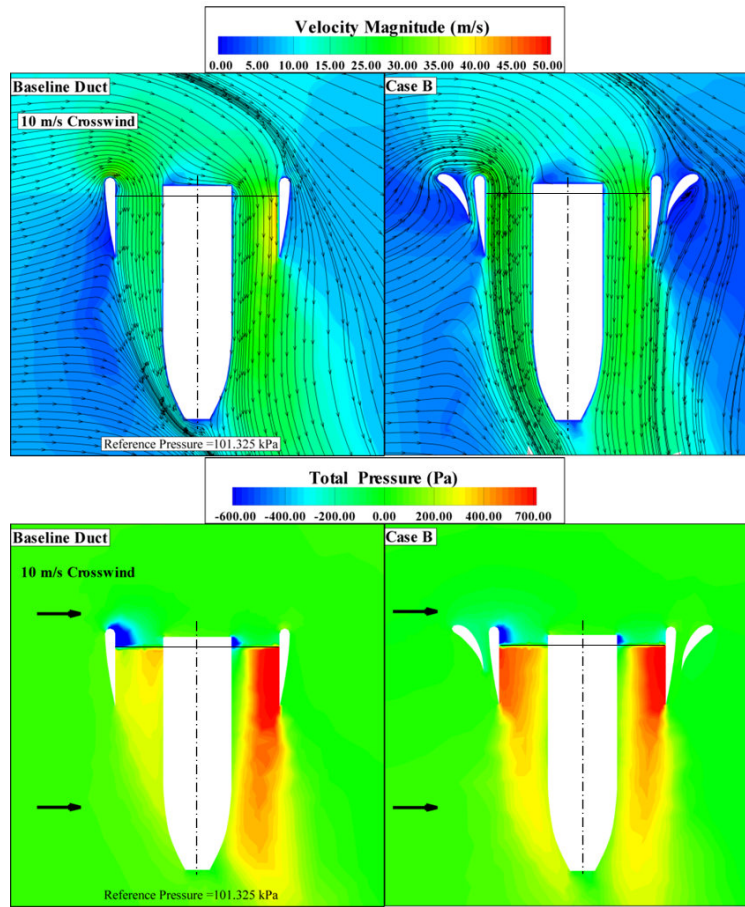
FIGURE 14: Velocity magnitude and total pressure distribution, baseline duct versus CASE-B short double ducted fan (DDF) at 10 m/s edgewise flight velocity
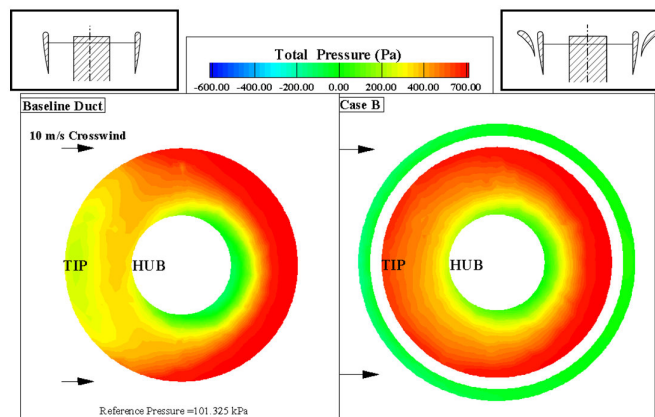

FIGURE 15: Total pressure distribution at rotor exit plane (horizontal) baseline duct versus CASE-B short double ducted fan (DDF) at 10 m/s edgewise flight velocity
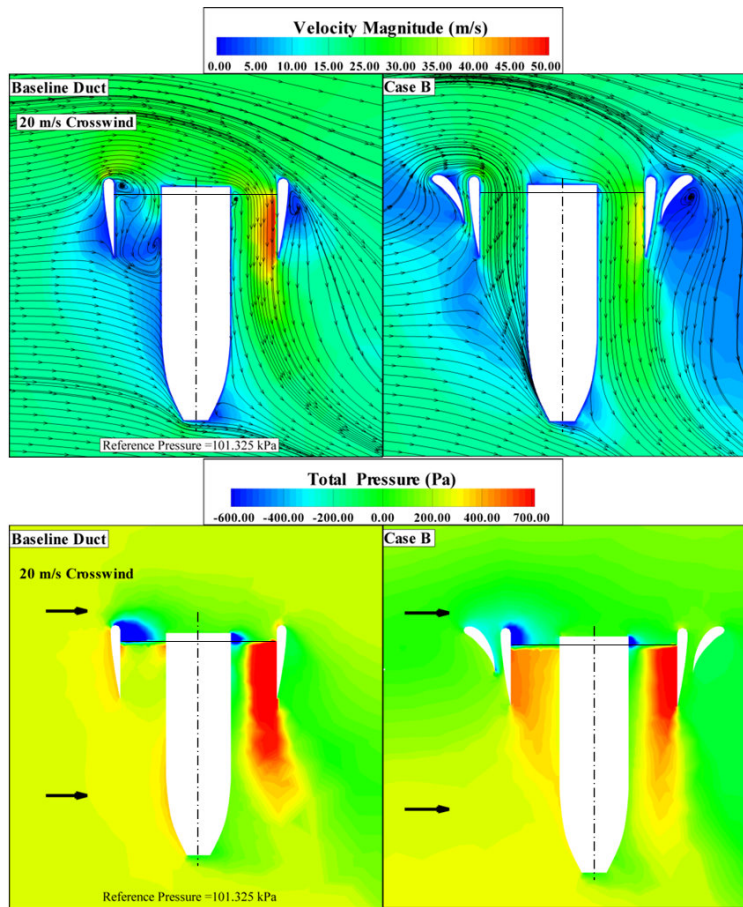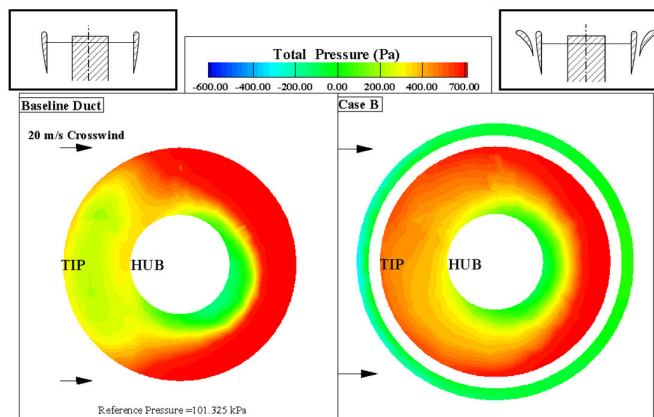
FIGURE 16: Velocity magnitude and total pressure distribution, baseline duct versus CASE-B short double ducted fan (DDF) at 20 m/s edgewise flight velocity

FIGURE 17: Total pressure distribution at rotor exit plane (horizontal) baseline duct versus CASE-B short double ducted fan (DDF) at 20 m/s edgewise flight velocity
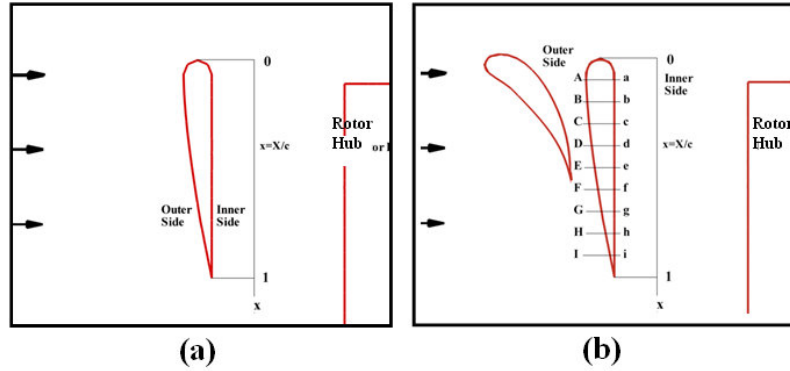
FIGURE 18: Sampling locations for static pressure and skin friction coefficient computations near the leading side of the inner duct for (DDF) CASE-B
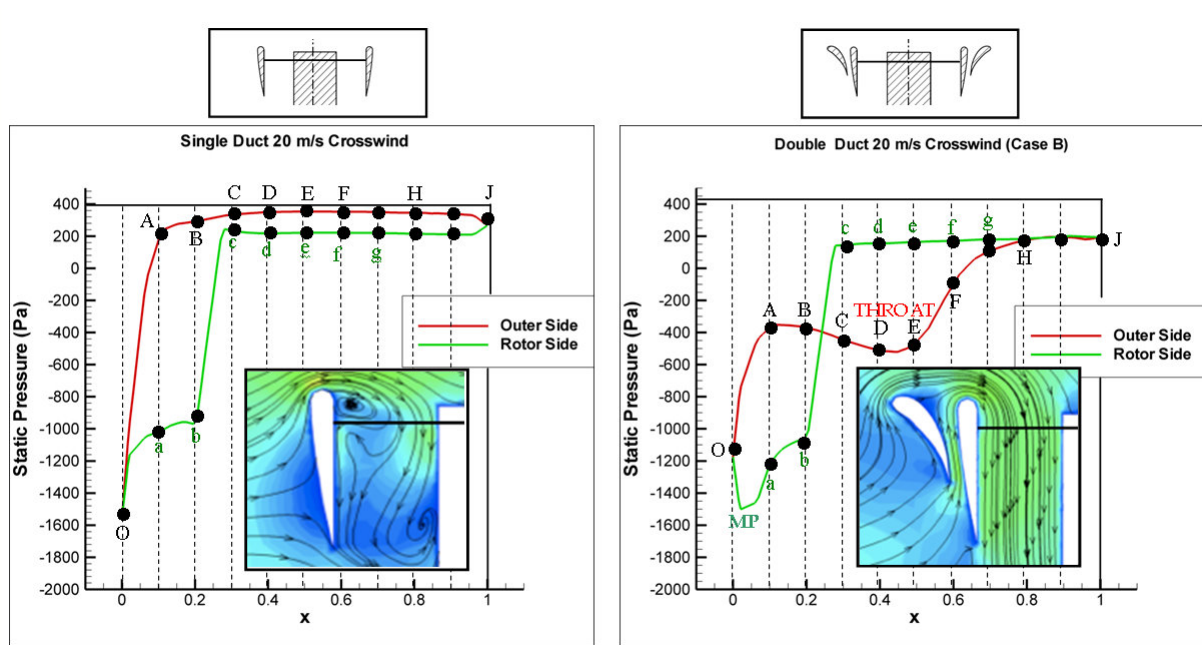

FIGURE 19: Comparison of the static pressure distribution on the baseline lip section and inner duct lip section of the (DDF) CASE-B airfoil

The vertically upward channel flow in the outer duct section is established by the dynamic pressure of the external flow in edge-wise flight. The vertically upward flow exists in a narrow leading edge region as clearly shown in Figure 16 and the results showing the axial velocity vectors from the computations. The outer duct flow that is proceeding vertically up generates a unique wall static pressure distribution in a converging-diverging channel. The external flow in horizontal flight stagnates on the shorter outer airfoil and turns upward towards the leading edge of the outer duct airfoil. Most of the flow stagnating at the lower part of the vehicle is directed towards the converging diverging chan-

nel of the outer duct. There is a wide stagnation region between points J and H on the outer side of the inner duct. The flow accelerates towards the throat section of the outer duct near D. The flow after the throat section smoothly decelerates up to the point A that is very close to the leading edge circle of the leading edge. The existence of the diverging channel is responsible from a much softer acceleration around the leading edge diameter of the lip section between A and O. The flow is still accelerating when it is passing through the geometrical leading edge point O. The minimum pressure point (MP) in (DDF) configuration is on the inner side of the lip section at x=X/c=0.03 in contrary to

the baseline duct location O. The flow starts decelerating after this minimum pressure point MP. The adverse pressure gradient region after the minimum pressure point MP in (DDF) is much shorter and the adverse pressure gradient between MP and a is much milder than that of the baseline duct. Figure 19 clearly shows the favorable modified nature of the static pressure distribution around the lip section of (DDF) leading to the elimination of the severe inlet lip separation region that is unique to the baseline duct in edgewise flight. The (DDF) approach is extremely useful in controlling the inner lip flow separation originating the adverse pressure gradient region.

9 SUMMARY AND CONCLUSIONS

This paper describes a novel ducted fan inlet flow conditioning concept that will significantly improve the performance and controllability of VTOL "*vertical take-off and landing*" vehicles, UAVs "*uninhabited aerial vehicles*" and many other ducted fan based systems. The new (DDF) concept developed in this study deals with most of the significant technical problems in ducted fans operating at almost 90° angle of attach, in the edgewise flight mode. The technical problems related to this mode of operation are as follows:

Increased aerodynamic losses and temporal instability of the fan rotor flow when "*inlet flow distortion*" from "*the lip separation area*" finds its way into the tip clearance gap leading to the loss of energy addition capability of the rotor.

Reduced thrust generation from the upstream side of the duct due to the rotor breathing low-momentum re-circulatory turbulent flow.

A severe imbalance of the duct inner static pressure field resulting from low momentum fluid entering into the rotor on the leading side and high momentum fluid unnecessarily energized on the trailing side of the rotor.

A measurable increase in power demand and fuel consumption when the lip separation occurs to keep up with a given operational task.

Lip separation and its interaction with the tip gap flow requires a much more complex vehicle control system because of the severe non-uniformity of the exit jet in circumferential direction and excessive pitch-up moment generation.

At low horizontal speeds a severe limitation in the rate of descent and vehicle controllability may occur because of more pronounced lip separation. Low power requirement of a typical descent results in a lower disk loading and more pronounced lip separation.

Excessive noise and vibration from the rotor working with a significant inlet flow distortion.

Very complex unsteady interactions of duct exit flow with control surfaces.

The new concept that will significantly reduce the inlet lip separation related performance penalties in the edgewise flight zone is named "*DOUBLE DUCTED FAN (DDF)*". The current concept development uses a time efficient 3D computational viscous flow solution approach developed specifically for ducted fan flows. The present study summarizes only the most optimal approach after evaluating nine different double ducted fan geometries for a wide range of edgewise flight velocities.

The current concept uses a secondary stationary duct system to control "*inlet lip separation*" related momentum deficit at the inlet of the fan rotor occurring at elevated edgewise flight velocities. The DDF is self-adjusting in a wide edgewise flight velocity regime.

DDFs corrective aerodynamic influence becomes more pronounced with increasing flight velocity due to its inherent design properties.

Case-B was the best DDF configuration designed. It has improved mass flow rate passing from the duct by 40 % and improved thrust force obtained from the ducted fan by 56.2 % relative to baseline duct in edgewise flight condition.

The DDF can also be implemented as a "*Variable Double Ducted Fan*" (VDDF) for a much more effective inlet lip separation control in a wide range of horizontal flight velocities in UAVs, air vehicles, trains, buses, marine vehicles and any axial flow fan system where there is significant lip separation distorting the inlet flow.

Most axial flow fans are designed for an inlet flow with zero or minimal inlet flow distortion. The DDF concept is proven to be an effective way of dealing with inlet flow distortions occurring near the tip section of any axial flow fan rotor system operating at high angle of attack.

ACKNOWLEDGMENT

REFERENCES

[1] Abrego, A. I., and Bulaga, R. W., 2002. "Performance study of a ducted fan system". *AHS Aerodynamics, Aeroacoustic , Test and Evaluation Technical Specialist Meeting*.

[2] Martin, P., and Tung, C., 2004. "Performance and flowfield measurements on a 10-inch ducted rotor vtol uav". *60th Annual Forum of the American Helicopter Society*.

[3] Graf, W., Fleming, J., and Wing, N., 2008. "Improving ducted fan uav aerodynamics in forward flight". *46th AIAA Aerospace Sciences Meeting and Exhibit*.

[4] Graf, W. E., 2005. "Effects of duct lip shaping and various

control devices on the hover and forward flight performance of ducted fan uavs". Master's thesis, Virginia Polytechnic Institute and State University, Blacksburg, Virginia, May.

[5] Kriebel, A. R., and Mendehall, M. R., 1966. "Predicted and measured performance of two full-scale ducted propellers". *CAL/USAAVLABS Symposium on Aerodynamic Problems Associated with V/STOL Aircraft, Vol II: Propulsion and Interference Aerodynamics*.

[6] Mort, K. W., and Gamse, B., 1967. A wind tunnel investigation of a 7-foot-diameter ducted propeller. Tech. Rep. NASA TND-4142.

[7] Mort, K. W., and Yaggy, P. F., 1962. Aerodynamic characteristics of a 4-foot-diameter ducted fan mounted on the tip of a semispan wing. Tech. Rep. NASA TND-1301.

[8] Yaggy, P. F., and Mort, K. W., 1961. A wind-tunnel investigation of a 4-foot-diameter ducted fan mounted on the tip of a semispan wing. Tech. Rep. NASA TND-776.

[9] Lind, R., Nathman, J. K., and Gilchrist, I., 2006. "Ducted rotor performance calculations and comparisons with experimental data". *44th AIAA Aerospace Sciences Meeting and Exhibit*.

[10] He, C., and Xin, H., 2006. "An unsteady ducted fan model for rotorcraft flight simulation". *62th AHS Forum*.

[11] Chang, I. C., and Rajagopalan, R. G., 2003. "Cfd analysis for ducted fans with validation". *21th AIAA Applied Aerodynamics Conference*.

[12] Ahn, J., and Lee, K. T., 2004. "Performance prediction and design of a ducted fan system". *40th AIAA/ASME/SAE/ASEE Joint Propulsion Conference and Exhibit*.

[13] Ko, A., Ohanian, O. J., and Gelhausen, P., 2007. "Ducted fan uav modeling and simulation in preliminary design". *AIAA Modeling and Simulation Technologies Conference and Exhibit*.

[14] Zhao, H. W., and Bil, C., 2008. "Aerodynamic design and analysis of a vtol ducted-fan uav". *26th AIAA Applied Aerodynamics Conference*.

[15] Camci, C., and Akturk, A., 2011. Double ducted fan. U.S. Patent Publ. Number 2011 0217163 A1.

[16] ANSYS, 2009. Ansys-fluent v12 user's guide.